Effect of ZrO_2 Additives on the Nanomechanical Properties of Spark Plasma Sintered 93WC/7-xCo/xZrO_2-2mol% Y_2O_3 Powders Prepared by High-Energy Ball Milling

M. Sherif El-Eskandarany, Abdulsalam Al-Hazza, Latifa Al-Hajji, Ahmed Alduweesh, Shuroug Ahmed and Aisha Al-Rowayeh

Nanotechnology and Advanced Materials Program,
Energy and Building Research Center, Kuwait Institute for Scientific Research
Safat 13109, Kuwait - State of Kuwait, msherif@kisr.edu.kw

ABSTRACT

A high-energy ball milling technique was employed to prepare nanocomposite powders with compositions (wt.%) of 93WC/7-xCo/xZrO_2-2mol% Y_2O_3 powders (x=0, 1, 2, 3, 4, 5, 6, 7 wt%). The nanocomposite powders obtained after 75 h of ball milling possessed excellent morphological characteristics with spherical morphology and an average powder particle size of 150 nm in diameter. The powder of the end-products, which consisted of fine grains with an average grain size of 8 nm in diameter, were then consolidated in vacuum under a uniaxial pressure of 30 MPa at 1250 °C using spark plasma sintering (SPS). The fully dense nanocomposite bulk samples obtained via the SPS process maintain their nanocrystalline structure and have an average size of 55–86 nm in diameter. The indentation fracture toughness (K_{c1}) of the bulk consolidated materials decreased with the increasing mole fractions of ZrO_2 and ranged from 8.83 to 15.48 MPa.$m^{1/2}$. The effet of ZrO2 additives on the nanohardness and elastic modulli of the fabricated bulk nanocomposite system were experimentally investigated and reported in this study.

Keywords: Nanotechnology, powder technology, mechanical ball milling, fracture toughness, nanoindentations

1 INTRODUCTION

The top-down approach [1] using the high-energy ball milling method [2] has been considered to be the most powerful technique for the synthesis homogeneous nanocomposite powders with controlled morphological properties [3]. Several dozens of nanocomposite systems have been fabricated using this technique [4]. Cemented carbides such as WC-Co composites are characterized by extraordinary hardness and wear resistance resulting from the high carbide content [5]. Co is usually used as binder to improve the sintering, strength and toughness of WC; however, the hardness and wear resistance of the cemented carbides are significantly reduced. Thus, using Co as binder limits the applications of WC-Co composites. The present work aims to study the effect of adding small concentrations (0 to 7 wt.%) of ZrO_2-2mol% Y_2O_3 nanocrystalline grains on improving the fracture toughness of mechanically mixed 93WC/7Co nanocomposite powders.

2 EXPERIMENTAL PROCEDURE

A 15-g of commercial WC powder (99.9%, 200 μm) was balanced and charged into a WC vial (45 ml in volume) and sealed together with five WC balls (10 mm in diameter) in a glove box under an argon gas atmosphere. The milling process was carried out for 20 h at room temperature using a high-energy mixer ball mill. The milling procedure was repeated 25 times in order to obtain approximately 350 g of ultrafine nanocrystalline WC powder for the preparation of WC-based nanocomposite materials. The as-ball-milled WC nanocrystalline powders obtained after 20 h of ball milling were mixed with different wt.% of metallic Co and ZrO_2-2 mol.% Y_2O_3 powders to yield the desired nominal composition of 93WC/7Co/xZrO_2-2mol% Y_2O_3 (x = 0, 1, 2, 3, 4, 5, 6 and 7 wt.%). The mixed powders of each ZrO_2-2 mol.% Y_2O_3 concentration were sealed in a cylindrical WC vial (250 ml in volume) together with 25 WC balls (10 mm in diameter) in a glove box under an argon gas atmosphere. The ball milling was carried out at room temperature for 75 h using a high-energy ball mill at a rotation speed of 250 rpm. The synthesized nanocomposite powders, were consolidated into full-dense bulk compacts, using vacuum-spark plasma sintering (SPS) machine operated at 1250°C with an applied uniaxial pressure of 30 MPa. The structural, morphological, and elemental compositions of all samples were investigated by means of x-ray diffraction (XRD), field emission high-resolution transmission electron microscopy (HRTEM) equipped with energy-dispersive X-ray spectroscopy (EDS), field emission scanning electron microscope (FESEM/EDS), atomic force microscopy (AFM). The microhardness of all of the consolidated samples was determined using the Vickers hardness test with a load of 20 kg. The fracture toughness of the consolidated samples was determined using the VHT indenter crack-length measurements approach. Nanoindentation was employed to determine the nanomechanical properties of the as-consolidated

nanocomposite samples using a nanoindenter with a diamond Berkovich-tip.

3 RESULTS AND DISCUSSIONS

The XRD pattern of nanocomposite 93WC/7ZrO_2-2 mol.% Y_2O_3 powders obtained after 75 h of HEBM is shown in Fig 1(a). The powders revealed Bragg peaks of two individual phases corresponding to hcp-WC and tetragonal-ZrO_2, without any undesired intermediate phase product(s). The Bragg peaks displayed significant broadening, suggesting the formation of nano-scaled grains. The FE-SEM micrograph of nanocomposite 93WC/7ZrO_2-2 mol.% Y_2O_3 powders obtained after 75 h of ball milling (end-product) is shown in Fig. 1(b). After this stage of ball milling, the powders consisted of uniform spheres with an average particle size of 86 nm in diameter.

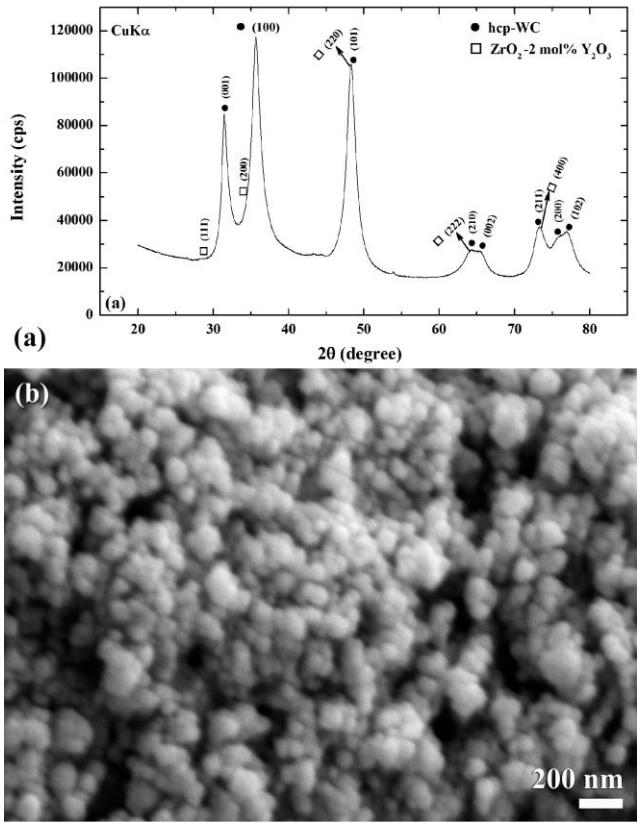

Figure 1: (a) XRD and (b) FE-SEM image of mechanically solid state mixed 93WC/7 wt.% ZrO_2-2mol Y_2O_3 nanocomposite powders obtained after ball milling for 75 h.

The HRTEM images of nanocomposite 93WC/4 wt.% Co/3 wt.% ZrO_2-2mol Y_2O_3 and 93WC/7 wt.% ZrO_2-2mol Y_2O_3 powders obtained after 75 h of HEBM are shown in Figs. 2(a) and 2(b), respectively. The locations of the constituent materials shown in Fig. 2 were determined by EDS dot-analysis and by measuring the d spacing of the lattice fingers that appeared in the grains. For both samples, nanocrystalline WC grains (less than 10 nm in diameter) were embedded and homogeneously distributed into the composite matrixes of Co/ZrO_2 (Fig. 2(a)) and ZrO_2 (Fig. 2(b)). No phase(s) other than the matrix elements and their reinforcement material could be detected. This dramatic decrease in the grain size can be attributed to the severe impact and shear forces generated by the milling tools, leading to continuous disintegration of the particles along their grain boundaries.

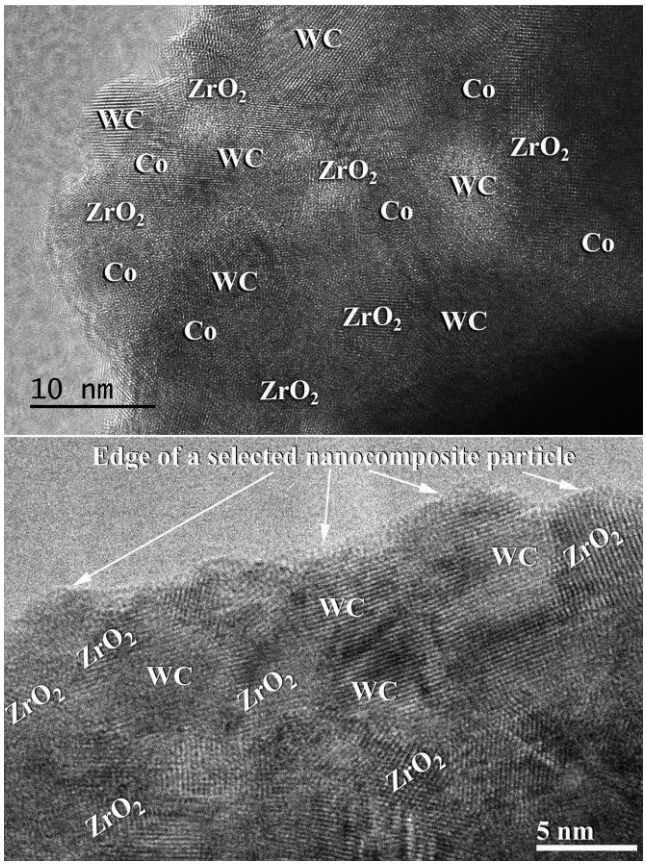

Figure 2: HRTEM images of mechanically solid state mixed (a) 93WC/4 wt.% Co/3 wt.% ZrO_2-2mol Y_2O_3 and (b) 93WC/7 wt.% ZrO_2-2mol Y_2O_3 nanocomposite powders obtained after ball milling for 75 h.

The bright field image (BFI) and the corresponding selected area diffraction pattern (SADP) of the bulk 93WC/7ZrO_2-2 mol.% Y_2O_3 nanocomposite are shown in Figs. 3(a) and 3(b), respectively. The as-consolidated material showed a highly dense and compact surface lacking voids and holes (Fig. 3(a)). The SPS engendered a slight grain growth and led to the production of larger grains with an average grain size ranging from 8 to 78 nm in diameter, as shown in Fig. 3(a). The SADP taken from the open circular region shown in Fig. 3(a), composed of hcp-WC and tetragonal-ZrO_2 phases, as elucidated in the indexed SADP (Fig. 3(b)). The theoretical bulk densities for the nanocomposite 93WC/7Co/x ZrO_2-2 mol.% Y_2O_3 were

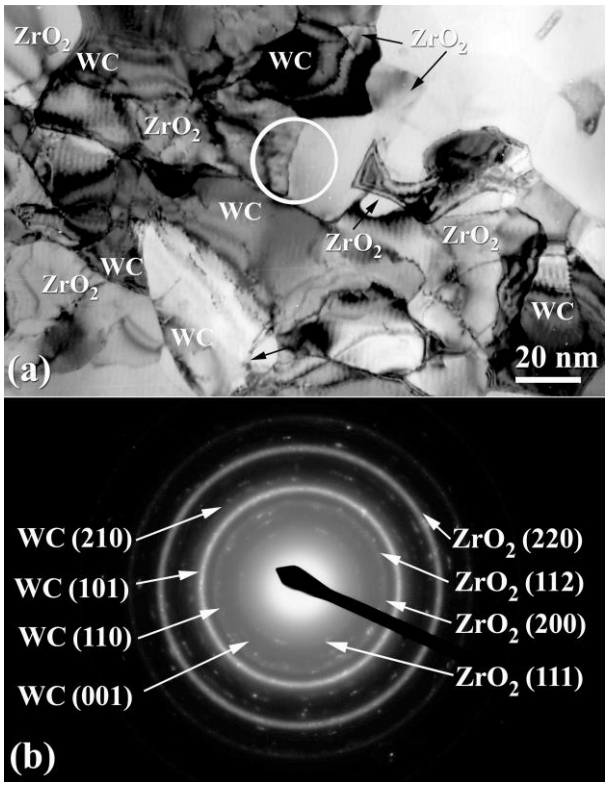

Figure 3: (a) BFI and (b) the corresponding SADP of as-consolidated 93WC/7 wt.% ZrO_2-2mol Y_2O_3 bulk nanocomposite.

calculated at different ZrO2 concentrations (x) using the rule of mixtures and are plotted in Fig. 4 along with the measured and relative densities. All of the consolidated samples had relative densities higher than 99.95 %, implying a full densification process that minimized the pore fractions in the consolidated samples. It can also be inferred from the

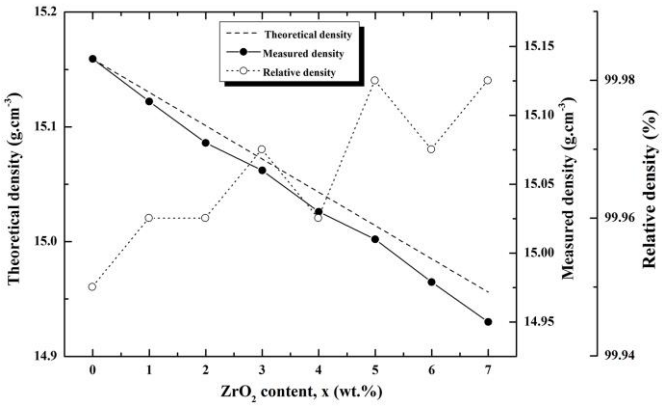

Figure 4: Calculated theoretical, measured and relative densities of the bulk 93WC/7Co/xZrO_2-2mol% Y_2O_3 nanocomposites with different ZrO_2 contents.

figure that increasing the volume fraction of ZrO_2 leads to a monotonical decrease in the bulk density of the nanocomposites. This is a natural consequence of replacing the high-density metallic Co (8.90 $g.cm^{-3}$) with ZrO_2-2mol% Y_2O_3 (6.0 $g.cm^{-3}$).

Figure 5 presents the relationships between nanohardness, nano-Young's modulus and the indentation depth of as-consolidated 93WC/7Co (Fig. 5(a)) and 93WC/7ZrO_2-2mol% Y_2O_3 (Fig. 5(b)) samples. The results showed that neither nanohardness nor Young's modulus varied dramatically from an examined zone to another, implying the absence of a serious compositional gradient at the micro-scale. The average values of nanohardness and Young's modulus obtained from at least 300 tests were found to be 19.67 GPa and 275 GPa for the 93WC/7Co sample and 19.26 GPa and 269 GPa for the 93WC/7ZrO_2-2mol% Y_2O_3 sample, respectively.

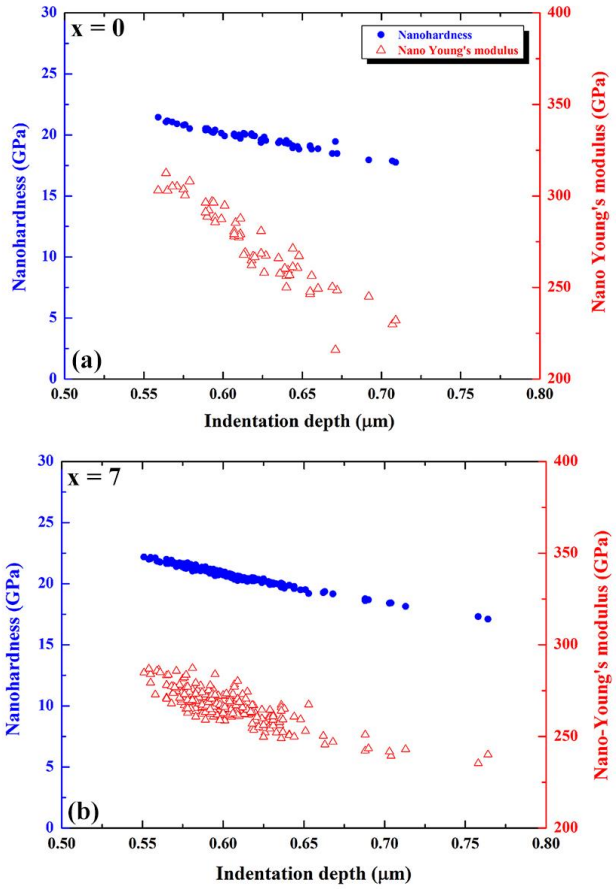

Figure 5: Dempence of nanohardness and nano-Yong's modulus on the ZrO2 additives for (a) x=0 and (b) x=7.

The FE-SEM micrograph of the bulk 93WC/7ZrO_2-2 mol% Y_2O_3 sample after the Vickers hardness test is shown in Fig. 6. The average length of the cracks demonstrated in the figure extended up to 74.8 μm from the indent, which indicates a K_{C1} value of 15.48 $MPa.m^{1/2}$. The multi-indents presented in Fig. 7(a) had nearly the same dimensions,

indicating the homogeneity in composition and nanomechanical properties of the bulk 93WC/7ZrO_2-2 mol% Y_2O_3 nanocomposite materials. The AFM micrograph of a single nanoindent taken at a higher magnification shows radial cracks around the nanoindent with ductile fracture, as presented in Fig. 7(b). The absence of sink-in behavior from the fractured surface can be seen. Sinking-in is expected in materials that exhibit a low value of E/Y (where E is the Young's modulus, and Y is the yield strength).

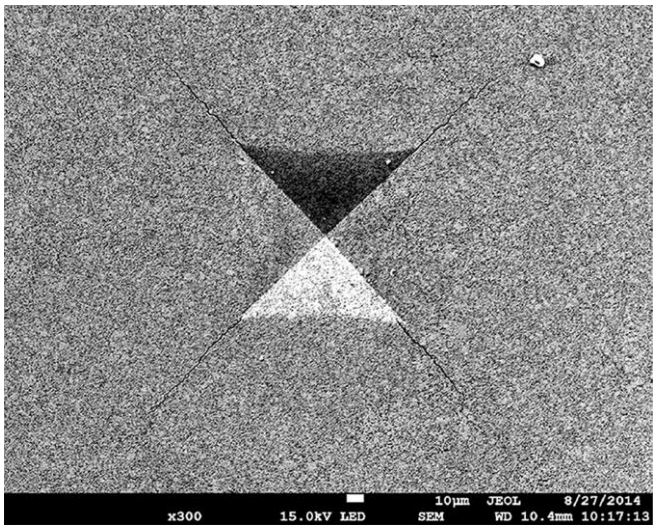

Figure 6: FE-SEM micrograph of a single Vickers indent (HV20) for bulk 93WC/7ZrO_2-2mol% Y_2O_3 nanocomposite.

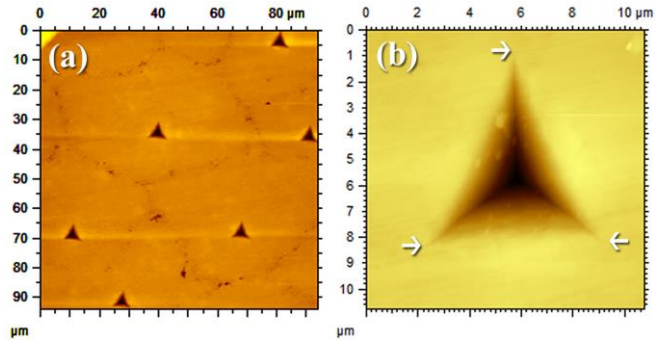

Figure 7: AFM images of selected nanoindents developed (a) on the surface micro- and (b) nano-radial cracks around the indents for bulk 93WC/7ZrO_2-2mol% Y_2O_3 nanocomposite.

Figure 8 shows the dependence of nanoindentations and fracture toughness on the ZrO_2 content plotted for nanocomposite 93WC/7Co/xZrO_2-2mol% Y_2O_3 bulk materials. The results showed that increasing the ZrO_2 content leads to a slight decrease in the nanohardness, which decreased from 19.67 GPa (for 93WC/7Co sample) to 19.26 GPa (for 93WC/7ZrO_2 sample). One can say that increasing the ZrO_2 content (x) may greatly improve the fracture toughness, as indicated by the monotonical increase in K_{C1} with the increase in the ZrO_2 contents. A maximum of 15.48 MPa.$m^{1/2}$ was achieved for 93WC/7ZrO_2 bulk nanocomposite. This value is far higher than the one calculated for 93WC/7Co (8.83 MPa.$m^{1/2}$). It should be emphasize that the addition of ZrO_2 nanograins increases the fracture toughness due to the transformation toughening.

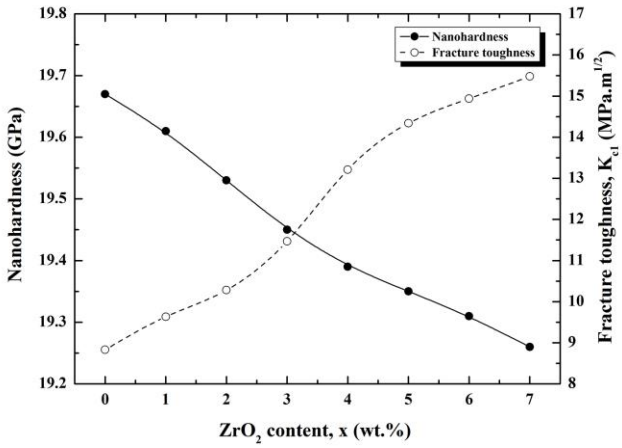

Figure 8: Dependence of nanohardness and fracture toughness on the ZrO_2 content for 93WC/7Co/xZrO_2-2mol% Y_2O_3 nanocomposite bulk materials.

4 CONCLUSIONS

A high-energy ball mill was employed to fabricate nanocomposite 93WC/7-xCo/xZrO_2-2mol% Y_2O_3 powders (x=0, 1, 2, 3, 4, 5, 6, 7 wt%) powders. The powders were consolidated into full-dense bulk compacts, using SPS technique. The effect of ZrO_2-2mol% Y_2O_3 additives on the mechanical properties of the nanocomposite system were investigated and reported.

REFERENCES

[1] M. Sherif El-Eskandarany, Journal of Nanoparticles, 2, 14-22, 2009.
[2] M Sherif El-Eskandarany, "Mechanical Alloying for Nanotechnology, Materials Science and Powder Metallurgy," 2nd ed., Elsevier Publishing, Oxford-UK, 2015, in press.
[3] M. Sherif El-Eskandarany, J. of Alloys Comp, 279, 263-271, 1998).
[4] C. Suryanarayana, and Nasser Al-Aqeeli, Progress in Materials Science, 58, 383-415, 2013.
[5] R. Raihanuzzaman, Z. Xie, S. J. Hong, and R. Ghomashchi, Powder Technology, 261, 1-8 2014.